Phase transition and magnetic anisotropy of $(La,Sr)MnO_3$ thin films

Zhi-Hong Wang[1,2,*] H. Kronmüller,[1] O. I. Lebedev,[3,†] G. M. Gross,[4] F. S. Razavi,[4] H. -U. Habermeier,[4] and B. G. Shen[2]
[1]*Max-Planck-Institut für Metallforschung, D-70569, Stuttgart, Germany*
[2]*State Key Laboratory of Magnetism, Institute of Physics and Center for Condensed Matter Physics, Chinese Academy of Sciences, Beijing 100080, China*
[3]*EMAT, University of Antwerp(RUCA), Groenborgerlaan 171, B-2020 Antwerp, Belgium*
[4]*Max-Planck-Institut für Festkörperforschung, D-70569, Stuttgart, Germany*
(Received 28 July 2001; published 8 January 2002)

The magnetic properties and their correlation with the microstructure and electrical transport are investigated in $La_{0.88}Sr_{0.1}MnO_3$ films grown on $(100)SrTiO_3$ single crystal substrates with thickness ranging from 100 to 2500 Å . The ultrathin film ($t=100$ Å) has a single ferromagnetic transition (FMT) at T_c of 250 K, whereas the thicker films exihibit two FMTs, with the main one at a lowered T_c of 200 K while the minor one around 300 K. Furthermore, a thickness dependent magnetic anisotropy has been found, strongly indicating the existence of strain effect, which is also revealed by the transmission electron microscopy study. The suppressed Jahn-Teller distortion (JTD) by the epitaxial strain, and the recovered JTD due to the strain relexation are suggested to explain the metallic behavior in thin films and the insulating behavior in the thick film ($t=2500$ Å), repectively.

DOI: 10.1103/PhysRevB.65.054411 PACS number(s): 75.70.−i, 75.60.−d, 73.50.−h, 68.37.−d

I. INTRODUCTION

The interplay between the structure, magnetism, and electrical transport of double exchange manganites $A_{1-x}A'_xMnO_3$ has attracted extensive studies. It has been established that the lattice effect imposed by the internal chemical or external hydrostatic pressure can profoundly modify the phase diagram.[1] Besides the double exchange between manganese spins, the Jahn-Teller splitting that localizes charge carriers in a local lattice distortion is very essential for a complete description of the evolved physics.[2] Due to the interest for application, considerable earlier work focused on growing thin films with large low field magnetoresistence.[3] Soon after, strain effects arising from the lattice mismatch between the substrate and the film were recognized to be important. Jin *et al.*, Kwon *et al.*, and Zandbergen *et al.* investigated the effect of strain on magnetoresistance of $La_{0.67}Ca_{0.33}MnO_3$, $La_{0.7}Sr_{0.3}MnO_3$, and $La_{0.73}Ca_{0.27}MnO_3$ thin films, respectively.[4–6] Wu *et al.* explored the magnetic domain structure in a compressively stressed $La_{0.7}Sr_{0.3}MnO_3$ film.[7] Several groups studied the magnetic anisotropy of thin film in tensile or compressive strain by torque magnetometry,[8] ferromagnetic resonance,[9,10] or magnetization measurements.[11–14] Millis *et al.*[15] and Shick[16] offered theoretical approaches on the strain issue in manganite thin films. In spite of those achievements, a full understanding of strain effect is still lacking. We note that most investigations on strain effects are carried out in films with a composition that is ferromagnetic (FM) metallic in the bulk phase diagram, whereas the work beyond the optimal doped regime ($x\sim 1/3$) is rather rare.

Very recently, a remarkable thickness dependent transport behavior was reported in $La_{0.88}Sr_{0.1}MnO_3$ thin films.[17] Namely, in the thick film of 2500 Å, a strong insulating behavior is found below the FM transition, which approaches the ground state of the corresponding bulk material. In contrast, as the film thickness decreases, a striking metallic state appears from the FM transition to low temperatures. It was suggested that the epitaxial strain had played a crucial role. In order to elucidate this point further, here we present a detailed study of magnetic properties as a function of thickness in the same thin films. Additionally, with investigation from the transmission electron microscopy (TEM), the correlation between the structure, magnetic properties, and transport behavior is clarified.

II. EXPERIMENT

Films of $La_{0.88}Sr_{0.1}MnO_3$ (LSMO) were grown on (100) $SrTiO_3$(STO) single crystal substrates at 760 °C by the standard pulsed laser deposition technique. To ensure a homogeneous oxygen stoichiometry, oxygen annealing for each film was performed at 900 °C for 1 h. The room temperature x-ray diffraction (θ-2θ scan) showed only (00l) reflections from film and STO, indicating a good texturation of the samples. Films with thicknesses of 100, 250, 500, 750, and 2500 Å were chosen for the present study. Magnetization was measured by a Quantum Design superconducting quantum interference device (SQUID) magnetometer. For a background subtraction, the magnetic moment of a blank (100) STO, the same as used for film growth, was measured. The surface morphology was observed by atomic force microscopy (AFM) on DI Nanoscope II. TEM studies, including high resolution microscopy (HREM) and electron diffraction (ED) by a Jeol 4000EX electron microscope, were carried out in cross-section specimens that are always with substrate.

III. RESULTS

Figure 1 shows the magnetization of the films as a function of temperature measured at 100 Oe. It is evident that the thin film with thickness of 100 Å has the highest Curie temperature (T_c) of 250 K. However, other films have a lower T_c around 200 K, indicating that the strain relaxation may

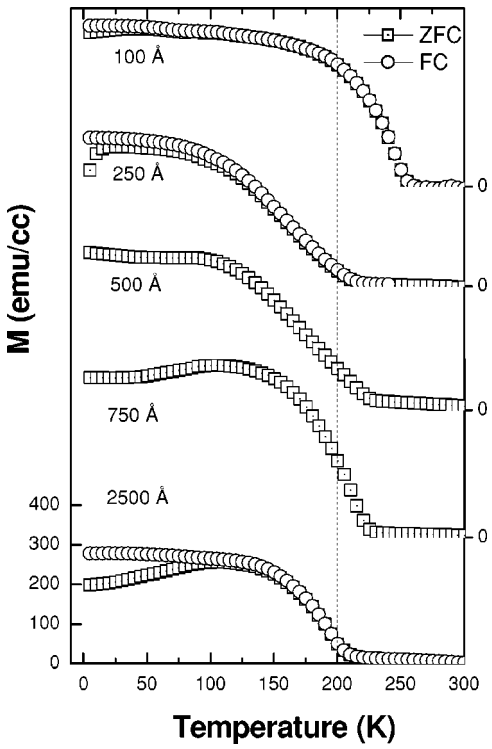

FIG. 1. Temperature dependence of magnetization measured with an in-plane field of 100 Oe. ZFC: zero-field-cooling, FC: field-cooling.

start when film thickness exceeds 100 Å. With increasing film thickness, the thermo-magnetization-irreversibility between zero-field-cooling and field cooling runs, arising from the spin disorder, becomes marked in the film of 2500 Å. In contrast to the film of 100 Å, the FM transition of thick films is broad, implying a distribution of exchange interaction strength, possibly induced by a structural disturbance. Thereafter, a further magnetization measurement from 200 to 300 K was undertaken with a smaller field of 50 Oe. Surprisingly, another minor FM transition around 300 K was found for all films except the thinnest one of 100 Å (see Fig. 2). The magnetization below the high T_c for the film of 250 Å has a bump near 250 K that is just the T_c for the 100 Å thin film. Furthermore, when the film becomes thick, the magnetization is found to be progressively increased. This intriguing phase separation behavior should be associated with a gradual strain relaxation.[18–20]

Magnetization hysteresis loops ($M-H$) were measured at 5 K with magnetic field along the three crystal orientations in a cubic STO index: [100], [110], and [001] (the measuring geometry is described in Fig. 3). Figure 4 displays the field dependence of the out-of-plane magnetization. Due to the demagnetization field, all films have a small remanence M_r in the [001] $M-H$ curves, showing an easy-plane magnetic anisotropy (MA). With increasing film thickness, the low-field magnetization rises more steeply with the external field (see the inset).

In Fig. 5, we show the field dependence of the in-plane magnetization. An in-plane biaxial MA was observed for films with thicknesses from 100 to 750 Å . Along the easy

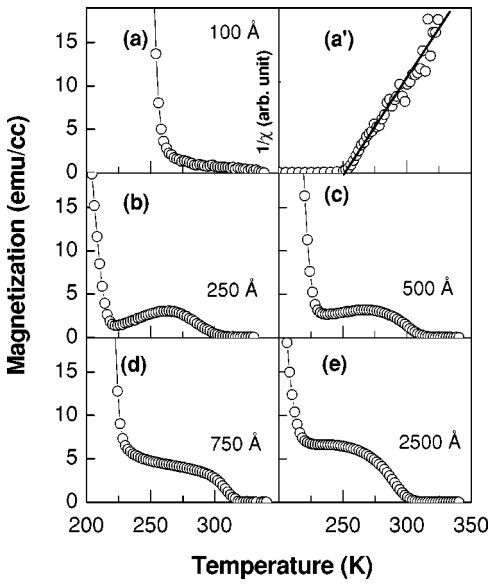

FIG. 2. Temperature dependence of magnetization measured with an in-plane field of 50 Oe in the high temperature region. (a′) shows the inverse susceptibility ($1/\chi$) vs temperature (T) for the thin film of 100 Å , a linear fit based on the Curie-Weiss law $\chi \sim 1/(T-T_C)$ indicates a single FM transition as well.

axis [110] for films of 250, 500, and 750 Å , a high remanence ratio M_r/M_s close to 1 was obtained. The ratio along [100] has a value around 0.7 that is very consistent with the $\cos(\pi/4)$ projection of the magnetic moment from the easy axis, demonstrating a good single crystalline quality of these samples. For the film of 100 Å, M_r/M_s along both [100] and [110] directions are a little lower, which leads to a less squared hystersis loop. For the film with 2500 Å , the loops in [100] and [110] are nearly overlapped, not showing the biaxial MA. This feature together with its substantially low M_r/M_s allow us to argue that the crystal orientation in the plane may have been lost in this thick film. With film thickness increasing from 100 to 750 Å , the coercive field reduces gradually from 52 to 10 Oe but increases again up to 55 Oe in the film of 2500 Å . This fact implies that the reversal of magnetization in thin films should be interpreted by a stress-governed mechanism, however, due to the strain

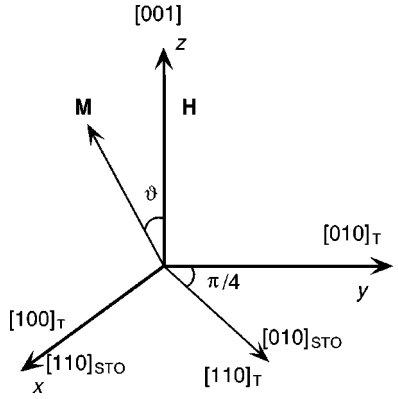

FIG. 3. The geometry of magnetization measurement, where the subscript T refers to the tetragonal symmetry.

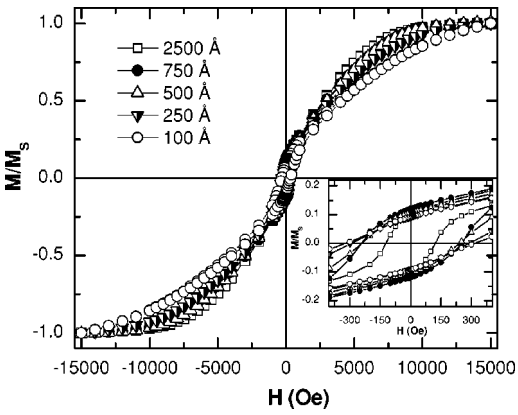

FIG. 4. Magnetization hysteresis loops measured along the [001] direction at 5 K. The inset shows the low field part.

relaxation it would be greatly affected by the numerous boundaries between the misorientated domains in the thick film ($t=2500$ Å).[21]

For shedding more lights on the thickness dependent magnetic properties, it is instructive to investigate the microstructure of these films. Figure 6 shows the low magnification multibeam diffraction TEM images taken from the cross-section specimens along a cube zone of STO. The thin film

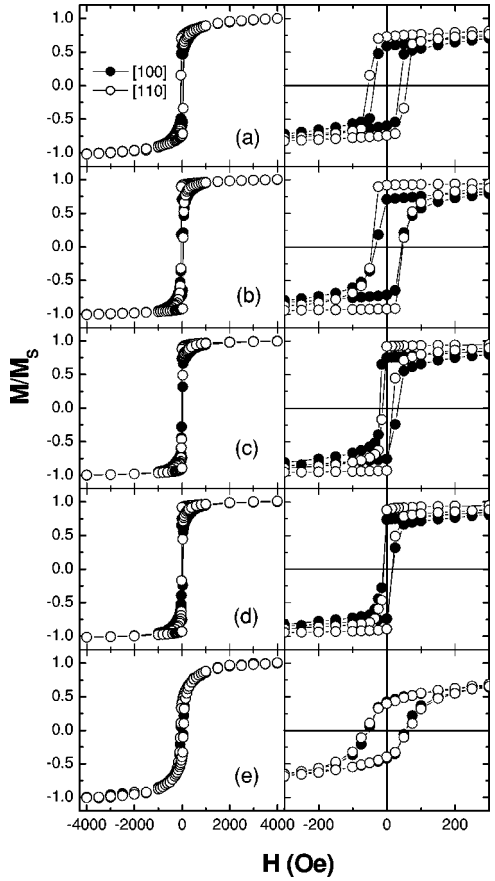

FIG. 5. Magnetization hysteresis loops measured along [100] and [110] directions at 5 K for films of (a) 100 Å, (b) 250 Å, (c) 500 Å, (d) 750 Å, and (e) 2500 Å. The right panels enlarge the low field part of the left ones.

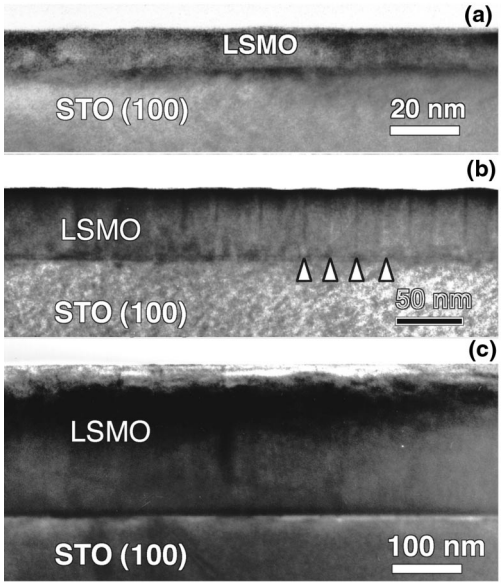

FIG. 6. Low magnification TEM images taken along a cube zone of STO of cross-section LSMO films with thickness of (a) 100 Å, (b) 500 Å, and (c) 2500 Å. The twin contrast in (b) is indicated by arrows.

($t=100$ Å) [Fig. 6(a)] has an uniform contrast showing neither domains nor intermediate layers inside. The HREM image of this film (Fig. 7) further provides the clear coherence of the lattice plane crossing the interface, close to which misfit dislocations were not detected. In addition, the excellent epitaxial growth, actually in a layer-by-layer mode were also revealed by the atomic terraces along the film surface (see the AFM image shown in Fig. 8). We propose that a surface-step-induced MA may account for the smaller squareness in the in-plane $M-H$ loop of this ultrathin film. Interestingly, as the film thickness increases to 500 Å , parallel bands were observed [Fig. 6(b)]. Further investigations indicate that they are produced by the periodic microtwinnings in orthogonally arranged macrodomains along [100] and [010].[22] We note that such domain orientation still allowed the observation of the biaxial MA and high remanence for this film. As displayed in Fig. 6(c), the thick film of 2500 Å does not show twin band contrast but owns a grainy textured microstructure.

Figure 9 shows the corresponding ED patterns recorded under the normal beam incidence along [100] or [010]. It

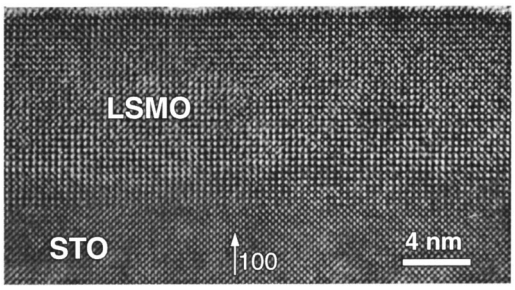

FIG. 7. HREM image for cross-section specimen of thin film with 100 Å taken along a cubic zone of STO.

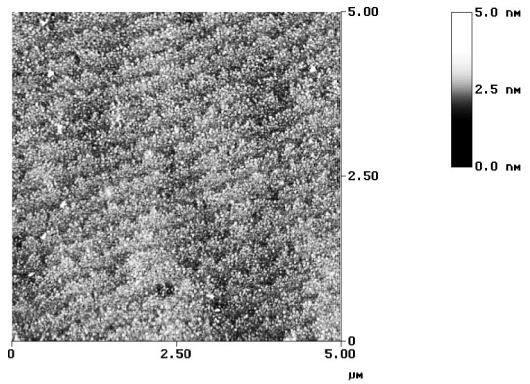

FIG. 8. AFM image of the thin film of 100 Å .

should be mentioned that the most intensive spots are from both film and substrate, while the weaker spots are only produced by the film. A single cube-zone ED pattern was observed in thin films ($t=100$ and 500 Å), and also in the film with thickness of 1000 Å.[22] In the film of 100 Å, the spots due to the film are slightly elongated along [001], suggesting a tetragonal distortion in this direction. In the film of 500 Å, the splitting in the spots due to the film is marked along the film plane, which is caused by the coherent twins. In the thick film ($t=2500$ Å), however, spots characteristic of the orthorhombic structure (Pbnm) owned by the corresponding bulk material have been found. Moreover, besides the [001] orthorhombic variant the [110] variant was ever observed [see Fig. 9(c)], which indicates the existence of grains with c-axis lying in the film plane, and well agrees with the in-plane magnetizing behavior of this film. We note that, because of the near degeneracy between the interplane spacing d_{002} and d_{110} in the orthorhombic structure, it is impossible to distinguish the second orientation from the earlier x-ray θ-2θ scan.

IV. DISCUSSION

The microstructure development has clearly shown that the ultrathin film ($t=100$ Å) should be coherently strained, however, the epitaxial strain has already partially relaxed at the thickness of 500 Å through the microtwinning pathway. It confirms the analysis based on the main FM transitions. The large structural disturbance in thick films, giving rise to the broad main FM transition and the marked spin disorder, is reasonably ascribed to the boundaries of the macrodomains or grains. In comparison with the single FM transition for the film of 100 Å , the simultaneous presence of an enhanced T_c (the minor high FM transition) and a lowered T_C (the main FM transition) in thick films, indicates that the minor high FM phase should be attributed to the few layers close to the substrate, where the strain is still coherently imposed and may be even strengthened due to the average reduction of strain in the whole layers. Being consistent with this argument, according to the magnetization measurements (see Fig. 1) the fraction of the secondary phase is known to be rather small (less than 1%). We propose that, the not fully relaxed strain state even for the thickest film ($t=2500$ Å), may be attributed to the difficulty of dislocations to migrate in this strongly bonded system.

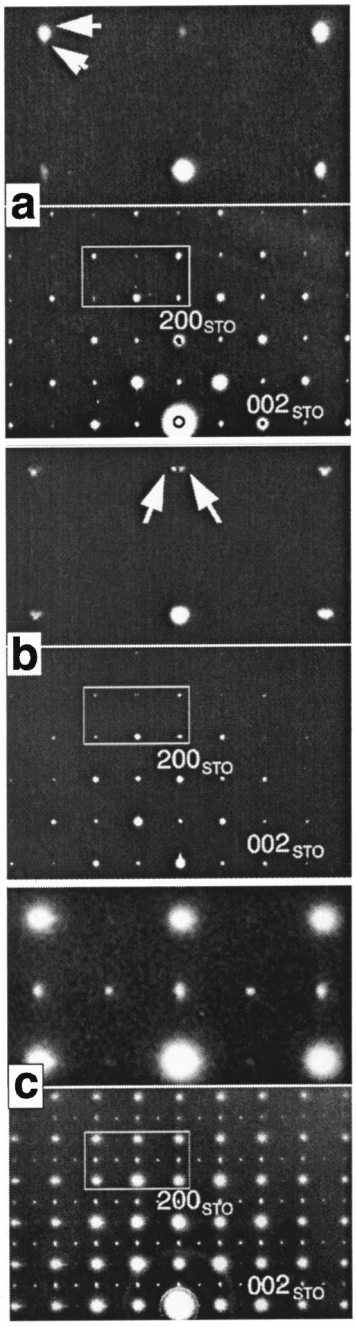

FIG. 9. ED patterns taken along a cube zone of STO of cross-section specimens for films with thickness of (a) 100 Å, (b) 500 Å, and (c) 2500 Å. The marked square image is enlarged in each top panel. The arrows in (a) indicate the elongation along [001], in (b) indicate the splitting along the film plane (see the context).

Using the $M-H$ data, we perform a further quantitative analysis. The total free energy E can be expressed by the same tetragonal symmetry for the films studied here[23]

$$E=K_1m_z^2+K_2m_z^4+K_3m_x^2m_y^2-\mathbf{M}\cdot\mathbf{H}+2\pi M^2m_z^2, \quad (1)$$

where K_1 and K_2 are the second and fourth order uniaxial anisotropy constants, respectively. K_3 is the in-plane biaxial

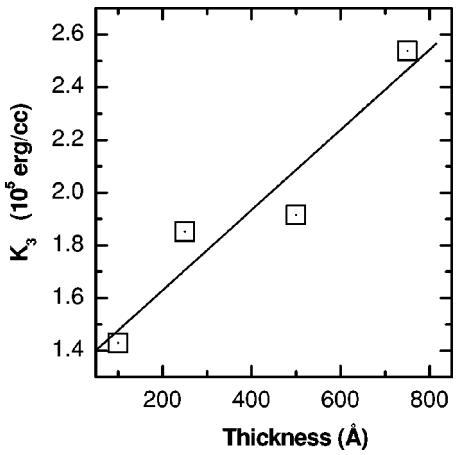

FIG. 10. Thickness dependence of the biaxial magnetic anisotropy constant K_3. The solid line is guide to eye.

anisotropy constant, $m_{x,y,z}$ are the direction cosines of the magnetization vector **M**, and the last term represents the thin film demagnetization energy $N_d M^2 m_z^2/2$ (demagnetizing factor $N_d = 4\pi$). Taking the data shown in Fig. 5, the in-plane MA energy difference between [100] and [110] can provide an evaluation of $K_3 = 4(E_{[100]} - E_{[110]}) = 4(\int_{[100]}^{M_s} - \int_{[110]}^{M_s}) H\, dM$. On the other hand, when **H** is applied along [001], **M** will coherently rotate from the $[110]([100]_T)$ to the z axis (see Fig. 3). In this process the term $K_3 m_x^2 m_y^2$ is always zero. Minimizing Eq. (1) by $\partial E/\partial\theta = 0$ yields the equilibrium magnetization M in the H direction,

$$H = \left(\frac{2K_1}{M_s^2} + 4\pi \right) \cdot M + \frac{4K_2}{M_s^4} \cdot M^3. \qquad (2)$$

$K_{1,2}$ can be derived from the linear regression between H/M and M^2 by the method of least squares. The MA energy difference ΔE_{aniso} between [001] and [110], and the MA field H_K (shape anisotropy free), are then given by $\Delta E_{\text{aniso}} = K_1 + K_2$, and $H_K = 2(K_1 + 2K_2)/M_s$, respectively.

As shown in Fig. 10, the obtained K_3 is found to increase with film thickness, indicating a larger lattice distortion in the plane for thicker films. This trend is expected to be remained for the thick film (t=2500 Å) if K_3 could be available from a sample with single crystal nature. Since the film of 2500 Å is not perfectly [001]-textured, we present only the calculated values of ΔE_{aniso} and H_K for the other four films in Fig. 11. The inset shows the found good linear relation between H/M and M^2. The upper deviation from the linearity occurs as M approaches saturation, while the lower deviation is due to the magnetic domain effects, or in other words, **M** does not rotate coherently in this low field regime. It can be seen that, with increasing film thickness, the positive ΔE_{aniso} turns to be negative while H_K decreases. This result clearly demonstrates that the thick film tends to *regain the intrinsic perpendicular* MA, whereas the thin film has a strain induced *in-plane* MA.

Note that the magnetoelastic coupling energy is given by $E_\sigma = 3/2\lambda\sigma$, where λ is the magnetostriction coefficient, and σ is the imposed *in-plane stress*.[24] The strain-induced in-

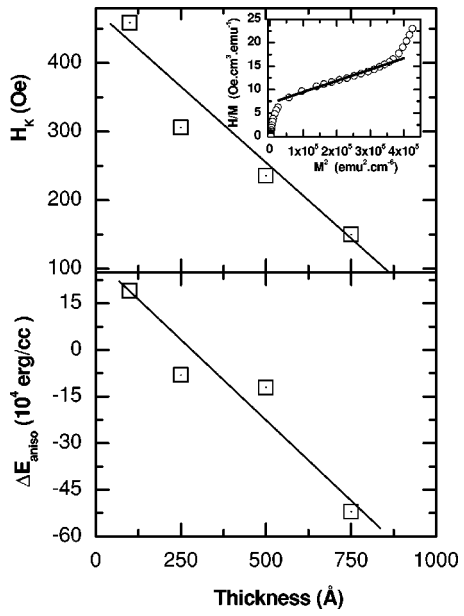

FIG. 11. Thickness dependence of (a) magnetic anisotropy field H_K in [001], and (b) MA energy difference ΔE_{aniso} between [001] and [110]. The solid lines are guides to eye. The inset illustrates H/M vs M^2 for the thin film of 250 Å, a linear fit is shown.

plane MA therefore implies $\lambda\sigma > 0$. Further, the low temperature λ is positive for $La_{1-x}Sr_xMnO_3$ single crystals,[25] indicating that the stress imposed by the substrate should be tensile along the film plane (and accordingly, the resulted stress along [001] is compressive). It can be learned from Fig. 11 that the magnetocrystalline energy ΔE_{aniso} for the corresponding bulk material should exceed 5.2×10^5 erg/cm^3 more or less, and then the strain contributed magnetoelastic energy larger than $\sim 7.1 \times 10^5$ erg/cm^3 can be obtained for the thin film of 100 Å. For the present low Sr doped LSMO, λ is around 1×10^{-5} at 5 K.[25] As a result, the acting stress not less than 4.7 GPa and $dT_c/d\sigma \leqslant 11$ K/GPa are evaluated for the thin film of 100 Å . It is noteworthy that a little larger dT_c/dP with magnitude of 20–30 K/GPa is realized by the hydrostatic pressure (P) in the corresponding bulk material.[26]

The pseudocubic symmetry of the ultrathin film ($t = 100$ Å) under a tensile stress suggests that observed FM metallic state with an enhanced T_c should not arise from the variance of the Mn–O bond length, but the less Jahn-Teller distorted MnO_6 octahedra due to the epitaxial strain. On the other hand, as reflected by the observed orthorhombic structure in the thick film ($t = 2500$ Å), the recovered Jahn-Teller distortion because of the strain relaxation would weaken the double exchange between Mn spins and consequently lead to the charge localization. The macrodomain or grain boundaries (GB) enables the additional electron scattering. Nevertheless, they can not be the origin of the insulating state in the thick film ($t = 2500$ Å), if keeping the GB of a metallic polycrystalline manganites in mind. Furthermore, it is worthwhile to point out that if film is grown from FM metallic target that usually has a high structural symmetry in the optimal doping range ($x \sim 1/3$), a reduction in T_c and a tendency for insulating state will be found for very thin

films no matter the imposed strain is tensile or compressive.[20,27] We suggest that the epitaxial strain lowering the high structure symmetry by enhancing the Jahn-Teller distortion should be responsible for the reverse strain effects as compared with the present case in the low Sr doped regime.

V. CONCLUSION

The phase transition, magnetic anisotropy, and their intimate correlation with the microstructure and electrical transport have been investigated for LaSrMnO thin films grown on (100) $SrTiO_3$ single crystals. Strong evidence shows that it is the epitaxial strain that suppresses the Jahn-Teller distortion, and consequently, induces the huge difference in structure, magnetic, and transport properties between the thin film and the thick film. As demonstrated in the present study, a modification of the Jahn-Teller distortion by a coherently imposed or partially relaxed strain can be used as an effective tool to tailor the physical properties of perovskite manganite.

ACKNOWLEDGMENTS

It is a pleasure for Z.H.W. to thank S. Fischer for her kind help in the experiments. This work was supported by the Joint Program between MPG (Germany) and CAS (China), and the State Key Project for Fundamental Research of China. Part of this work was also performed within the framework of IUAP 4/10 of the Belgian government.

*Corresponding author. Current address: Max-Planck-Institut für Festkörperforschung, Heisenbergstr. 1, D-70569, Stuttgart, Germany.

†On leave from Institute of Crystallography RAS, Leninsky pr. 59, 117333, Moscow, Russia.

[1] J. J. Neumeier, M. F. Hundley, J. D. Thompson, and R. H. Heffner, Phys. Rev. B **52**, R7006 (1995); H. Y. Hwang, T. T. Palstra, S.-W. Cheong and B. Batlogg, *ibid.* **52**, 15 046 (1995); H. Y. Hwang, S.-W. Cheong, P. G. Radelli, M. Marezio, and B. Batlogg, Phys. Rev. Lett. **75**, 914 (1995).

[2] A. J. Millis, Nature (London) **392**, 147 (1998).

[3] B. Mercey, J. Wolfman, and B. Raveau, Curr. Opin. Solid State Mater. Sci. **4**, 24 (1999), and references therein.

[4] S. Jin, T. H. Tiefel, M. McCormack, and H. M. O'Bryan, L. H. Chen, R. Ramesh, and D. Schurig, Appl. Phys. Lett. **67**, 557 (1995).

[5] C. Kwon, M. C. Robson, K.-C. Kim, J. Y. Gu, S. E. Lofland, S. M. Bhagat, Z. Trajanovic, M. Rajeswari, T. Venkatesan, A. R. Kratz, R. D. Gomez, and R. Ramesh, J. Magn. Magn. Mater. **172**, 229 (1997).

[6] H. W. Zandbergen, S. Freisem, T. Nojima, and J. Arts, Phys. Rev. B **60**, 10 259 (1999).

[7] Y. Wu, Y. Suzuki, U. Rüdiger, J. Yu, A. D. Kent, T. K. Nath, and C. B. Eom, Appl. Phys. Lett. **75**, 2295 (1999).

[8] Y. Suzuki, H. Y. Hwang, S.-W. Cheong, and R. B. van Dover, Appl. Phys. Lett. **71**, 140 (1997).

[9] S. E. Lofland, S. M. Bhagat, H. L. Ju, G. C. Xiong, T. Venkatesan, R. L. Greene, and S. Tyagi, J. Appl. Phys. **79**, 5166 (1996).

[10] L. B. Steren, M. Sirena, and J. Guimpel, J. Appl. Phys. **87**, 6755 (2000).

[11] T. K. Nath, R. A. Rao, D. Lavric, C. B. Eom, L. Wu, and F. Tsui, Appl. Phys. Lett. **74**, 1615 (1997).

[12] J. O'Donnell, M. S. Rzchowski, J. N. Eckstein, and I Bozovic, Appl. Phys. Lett. **72**, 1775 (1998).

[13] F. Tsui, M. C. Smoak, T. K. Nath, and C. B. Eom, Appl. Phys. Lett. **76**, 2421 (2000).

[14] X. W. Wu, M. S. Rzchowski, H. S. Wang, and Q. Li, Phys. Rev. B **61**, 501 (2000).

[15] A. J. Millis, T. Darling, and A. Migliori, J. Appl. Phys. **83**, 1588 (1998).

[16] A. B. Schick, Phys. Rev. B **60**, 6254 (1999).

[17] F. S. Razavi, G. Gross, H.-U. Habermeier, O. Lebedev, S. Amelinckx, G. Van Tendeloo, and A. Vigliante, Appl. Phys. Lett. **76**, 155 (2000).

[18] Y. Knoishi, M. Kasai, M. Kawasaki, and Y. Tokura, Mater. Sci. Eng., B **56**, 158 (1998).

[19] O. I. Lebedev, G. Van Tendeloo, S. Amelinckx, H. L. Ju, and M. Krishnan, Philos. Mag. A **80**, 673 (1999).

[20] S. I. Khartsev, P. Johnsson, and A. M. Grishin, J. Appl. Phys. **87**, 2394 (2000).

[21] Allan H. Morrish, *The Physical Principles of Magnetism* (Wiley, New York, 1965), p. 385.

[22] O. I. Lebedev, G. Van Tendeloo, S. Amelinckx, F. Razavi, and H.-U. Habermerier, Philos. Mag. A **81**, 797 (2001).

[23] L. D. Landau, E. M. Lifshitz, and L. P. Pitaevskii, *Electrodynamics of Continuous Media*, 2nd ed. (Butterworth Heinemann, Oxford, 1995), p. 138.

[24] B. D. Cullity, *Introduction to Magnetic Materials* (Addison-Wesley, Reading, MA, 1972).

[25] Yu. F. Popov, A. M. Kadomtseva, G. P. Vorob'ev, V. Yu. Ivanov, A. A. Mukhin, A. K. Zvedin, and A. M. Balbashov, J. Appl. Phys. **83**, 7160 (1998).

[26] Y. Moritomo, A. Asamitsu, and Y. Tokura, Phys. Rev. B **51**, 16 491 (1995); J.-S. Zhou, J. B. Goodenough, A. Asamitsu, and Y. Tokura, Phys. Rev. Lett. **79**, 3234 (1997); B. Martínez, R. Senis, Ll. Balcells, V. Laukhin, J. Fontcuberta, L. Pinsard, and A. Revcolevschi, Phys. Rev. B **61**, 8643 (2000).

[27] H. L. Ju, K. Krishnan, and D. Lederman, J. Appl. Phys. **83**, 7073 (1998); J. F. Bobo, D. Mahnoux, R. Porres, B. Raquet, J. C. Ocusset, A. R. Fert, Ch. Roucau, P. Bauls, M. J. Casanove, and E. Snoeck, *ibid.* **87**, 6773 (2000).